Research Article

Gokila Viswanathan, Ayyappan Solaiappan*, Brindha Thirumalairaj, Umapathi Krishnamoorthy*, Natrayan Lakshmaiya, Md Irfanul Haque Siddiqui, Mohd Asif Shah*

Improved photocatalytic properties of WO_3 nanoparticles for Malachite green dye degradation under visible light irradiation: An effect of La doping

https://doi.org/10.1515/chem-2024-0035
received March 14, 2024; accepted April 22, 2024

Abstract: Doped materials have received substantial attention due to their increased usefulness in photocatalytic applications. Within this context, the present study was dedicated to investigating the potential of the precipitation technique for producing La-doped tungsten oxide (WO_3). To comprehensively characterize the synthesized La-doped WO_3, scanning electron microscopy and X-ray diffraction were judiciously employed. The focal point of the investigation encompassed an examination of the impact of varying La concentrations on multiple fronts: the photocatalytic activities (PCAs), as well as any associated structural and morphological modifications. This holistic approach aimed to uncover the intricate relationship between La incorporation and the resulting properties of the WO_3 matrix. Through the degradation of Malachite green dye within an aqueous medium, PCA of the La-doped WO_3 samples was quantitatively evaluated. Remarkably, over 180 min under irradiation of visible light irradiation, the achieved levels of dye degradation were remarkable, amounting to 81.165, 83.11, and 83.85% for the respective samples. These findings firmly underscore the potential of La-doped WO_3 as a proficient photocatalyst, particularly in color removal from wastewater. This study paves the way for enhanced wastewater treatment approaches by utilizing doped WO_3 materials.

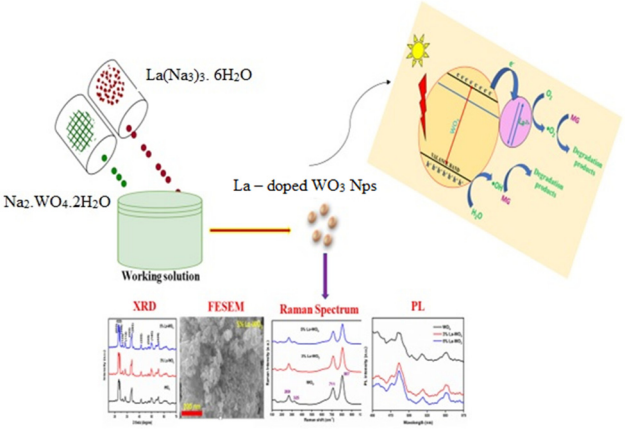

Graphical abstract

Keywords: tungsten oxide nanoparticles, lanthanum, malachite green, photocatalysis

1 Introduction

The contamination of pristine drinking water due to the improper disposal of industrial waste into waterways, wells, and lakes – sources primarily designated for human consumption. This contamination poses a significant threat

* **Corresponding author: Ayyappan Solaiappan**, Department of Physics, Government College of Engineering, Salem, 636011, India, e-mail: ayyappan@gct.ac.in
* **Corresponding author: Umapathi Krishnamoorthy**, Department of Biomedical Engineering, KIT-Kalaignarkarunanidhi Institute of Technology, Coimbatore, 641402, India, e-mail: umapathi.uit@gmail.com
* **Corresponding author: Mohd Asif Shah,** Department of Economics, Kebri Debar University, Somali, Ethiopia; University Centre for Research & Development, University School of Business, Chandigarh University, Gharuan, Mohali, Punjab, 140413, India, e-mail: drmohdasifshah@kdu.edu.et
Gokila Viswanathan: Department of Science and Humanities (Physics), Faculty of Engineering, Karpagam Academy of Higher Education, Coimbatore, 641021, India
Brindha Thirumalairaj: Department of Science and Humanities (Chemistry), KIT-Kalaignarkarunanidhi Institute of Technology, Coimbatore, 641402, India
Natrayan Lakshmaiya: Department of Mechanical Engineering, Saveetha School of Engineering, SIMATS, Chennai - 602105, Tamil Nadu, India
Md Irfanul Haque Siddiqui: Mechanical Engineering Department, College of Engineering, King Saud University, Riyadh 11451, Saudi Arabia, e-mail: msiddiqui2.c@ksu.edu.sa

to individuals and aquatic ecosystems, leading to detrimental consequences from consuming impure water. Pesticides, industrial chemicals, heavy metals, and other chemical contaminants can all be harmful to aquatic life. These contaminants can build up in living things' tissues, which can cause bioaccumulation and biomagnification in the food chain. In aquatic animals, they can cause genetic alterations, interfere with reproduction, compromise immune systems, and disturb physiological functions [1,2]. The endocrine system of aquatic species can be disrupted by specific chemical pollutants referred to as endocrine-disrupting chemicals (EDCs). EDCs cause disruptions to normal physiological processes such as growth, development, metabolism, and reproduction by mimicking or interfering with hormones. For instance, medications like birth control pills and estrogenic chemicals such as bisphenol A can feminize male fish and interfere with reproductive cycles of aquatic animals [3].

Many conventional methods, such as physical, chemical, and biological treatments, are effective in the removal of a diversified range of pollutants from wastewater. However, their efficiency depends on the type and concentration of contaminants. These methods are unique and can target various pollutants, including suspended solids, organic matter, nutrients, heavy metals, and pathogens. However, these methods are versatile; photocatalysis, particularly using advanced oxidation processes, has shown high efficiency in degrading organic pollutants, pathogens, and certain inorganic contaminants. This method is suitable for treating certain types of wastewater, particularly those containing organic pollutants susceptible to photocatalytic degradation. It may be more applicable in small applications or as a supplementary treatment step in combination with conventional methods [4,5]. It mineralizes all the organic compounds under suitable conditions. In this context, nanotechnology emerges as a revolutionary solution that holds the potential to address water-related challenges by surmounting technological barriers associated with the removal of contaminants from water sources. These contaminants encompass harmful metallic elements, dyes employed in the textile industry, chemical pesticides, and so on [6]. Numerous experts contend that nanotechnologies present more cost-effective, efficient, and robust pathways for crafting specific nanoparticles tailored for water treatment. This advancement could enable manufacturers to produce nanoparticles with reduced toxicity utilizing conventional methodologies. Notably, metal oxide (MO)-based semiconductor materials have assumed a pivotal role in a dynamic global market owing to their multifaceted characteristics and applications. Due to their intricate electron interactions, uncomplicated composition, and diverse stoichiometry, these materials serve as pivotal model compounds for unraveling the impacts of solid correlation in both physical and chemical phenomena. Furthermore, they have found wide-ranging utility across various applications, prominently in photocatalysis [7].

Photocatalysis is an advanced oxidation technique designed to tackle pressing environmental concerns, including air pollution and wastewater treatment from textile manufacturing. This innovative process hinges on the disintegration of organic compounds through the synergistic action of ultraviolet (UV) light and catalysts. The application of heterogeneous semiconductors as photocatalysts to disintegrate organic pollutants in water has recently garnered significant attention. Under the influence of light with energy greater than the semiconductor's band gap, an electron moves from the valence band (VB) to the conduction band (CB), resulting in positive holes within the VB. The formed positive holes instigate the production of hydroxyl radicals, renowned for their potent oxidation capabilities. These holes engage with dye molecules through a series of interactions, extracting electrons and thus initiating the breakdown process [8].

Furthermore, many semiconductors have found applications as photocatalysts in water remediation. MO nanoparticles, particularly TiO_2, ZnO, tungsten oxide (WO_3), CuO, and Cu_2O, have shown potential in water treatment due to their non-toxicity, stability, and cost-effectiveness [9,10]. Magnetic iron oxide/clay nanocomposites with high stability and adsorption capacities are also useful in water treatment applications [11]. Furthermore, the use of MO polymer nanocomposites has been investigated, with visible light response polymer/MO nanocomposites showing superior photodegradation activity against pollutants [12]. The successful immobilization of ultra-small cobalt oxide nanoparticles in MIL-101 and the role of MIL-101 in improving photocatalytic performance was investigated, and the practical approach of immobilizing catalyst nanoparticles on a suitable substrate using visible light-driven water oxidation reactions [13]. Nonetheless, their wide bandgap significantly curtails their efficacy when exposed to visible light [14]. Photocatalysis, a highly effective method for wastewater treatment, not only offers environmental safeguarding but also entails straightforward operation, an elevated mineralization rate, and potent oxidation potential, collectively facilitating the efficient elimination of low concentrations of organic contaminants from water sources [15]. WO_3 emerges as the best MO in the photocatalyst arena due to its comparatively small energy gap, elevated oxidation potential within the VB, and its adeptness in driving reactions under visible light illumination [16]. Beyond its role in photodegradation, WO_3 has exhibited various applications in antimicrobial actions and water splitting [17].

Nevertheless, a drawback inherent to WO_3 lies in its relatively lower CB, impeding its capacity to provide an appropriate potential for engaging with electron acceptors, consequently inciting electron–hole pair recombination [18]. To this end, the strategic modification of WO_3 through various techniques becomes imperative. Approaches such as meticulous morphological control, the construction of heterostructures, doping, and co-deposition with noble metals stand out as viable avenues to substantially enhance its photocatalytic prowess [19].

By surveying many reports related to this area, it came to our attention that, despite numerous studies focusing on the diverse applications of WO_3, there is either an absence or a minimal presence of articles concerning the co-precipitation synthesis of La-doped WO_3 nanoparticles for applications in optoelectronics and photocatalysis. This discovery left a remarkable impression on us, leading us to create La-doped WO_3 nanoparticles as a potent photocatalyst aimed at degrading hazardous Malachite green (MG) dye, and only a few articles reported the photocatalytic degradation of MG dye [20–22]. For instance, CuO nanoparticles were synthesized and tested for the photocatalytic degradation of MG dye using UV–Vis radiation [23]. Similarly, TiO_2 nanoparticles were synthesized by the microwave radiation method, and the absorption ability of MG dye was investigated [24]. Our study's core revolved around utilizing a straightforward co-precipitation method to synthesize WO_3 nanoparticles with La incorporation as a dopant. To comprehensively understand the impact of varying La concentrations, we meticulously investigated their influence on the crystal phase, particle size, morphology, and optical properties of the resultant WO_3 structures. A crucial phase of our research involved subjecting the synthesized nanomaterials to visible light irradiation, allowing us to assess their efficacy in the realm of photocatalysis through the degradation of MG dye. The insights gleaned from our research hold profound significance, particularly within the domain of water purification applications. By addressing the existing gap in knowledge and providing novel findings, our study contributes to the advancement of sustainable solutions for environmental concerns.

2 Experimental section

A diagrammatic representation for the synthesis of La-doped WO_3 nanoparticles is given in Scheme 1.

2.1 Source materials

Sodium tungstate dihydrate ($Na_2WO_4{\cdot}2H_2O$) and lanthanum (III) nitrate hexahydrate ($La(NO_3)_3{\cdot}6H_2O$), AR grade, were purchased from Sigma Aldrich. Hydrochloric acid (HCl) was bought from Nice Chemicals and used without further purification.

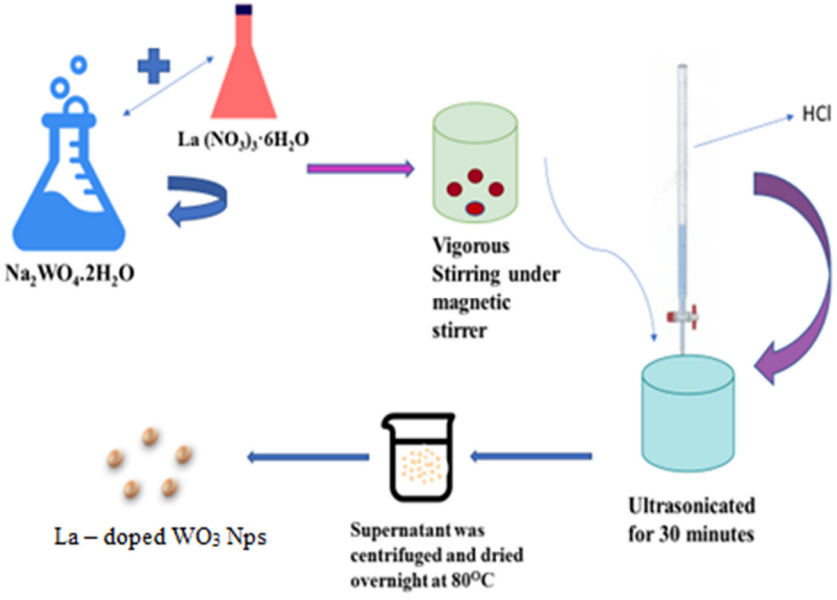

Scheme 1: Representation of synthesis of La-doped WO_3 nanoparticles.

2.2 Synthesis of La-doped WO_3 nanoparticles

For the synthesis of La-doped WO_3 nanoparticles, a simple co-precipitation method was adopted. About 7 mM of $Na_2WO_4{\cdot}2H_2O$ and different $La(NO_3)_3{\cdot}6H_2O$ were added to 50 mL of distilled water and stirred vigorously. The aforementioned solution was treated ultrasonically for 30 min. The pH of the solution was adjusted to one by adding 1 M HCl solution in drops. The supernatant was centrifuged and dried overnight at 80°C. Then, the grained powder was kept in a muffle furnace and calcinated at 450°C for 2 h.

2.3 Photocatalytic degradation of MG dye using La-doped WO_3 nanoparticles

La-doped WO_3 nanoparticles were used as a photocatalyst for the degradation of MG dye under UV–Vis irradiation. A 25 ppm MG dye was prepared, and 0.0001 g of La-doped WO_3 nanoparticles was added separately to 20 mL of the dye solution in 50 mL beakers. To reach the equilibrium, the solutions were kept in the dark for 30 min. Subsequently, the mixtures were exposed to UV–Vis light and stirred continuously for different durations of irradiation time. After irradiation, the photocatalyst nanoparticles were separated from the dye solution using a filtration process and centrifugation. Using a UV-visible spectrophotometer, the degradation of MG dye was monitored.

2.4 Characterization of La-doped WO_3 nanoparticles

X-ray diffraction (XRD) studies were carried out using XEPRT-PRO at λ = 1.5 Å with CuKα radiation. The Raman spectra were analyzed using a Jobin-Yvon T64000 spectrograph at room temperature. Morphological images were investigated using field emission-scanning electron microscopy (FE-SEM). UV–Vis spectroscopy (JASCO V-770 PC) was used to examine the optical absorption. A FluoroMax-4 fluorescence spectrophotometer was used to obtain the produced catalysts' photoluminous (PL) spectra.

3 Results and discussion

3.1 Structural features

3.1.1 XRD analysis

Figure 1 shows the crystalline configuration of the pure WO_3 and La-doped WO_3, encompassing a diverse series

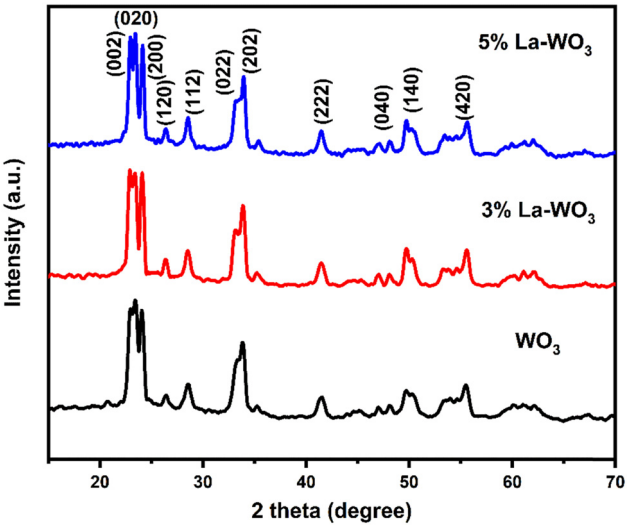

Figure 1: XRD pattern of pure WO_3 and La-doped WO_3 nanoparticles.

of molar ratios. Following the data extracted from the JCPDS No. 75-2187 reference, the diffraction peaks located at 22.9°, 23.5°, 24.2°, and 26.5° are unambiguously attributed to the (002), (020), (200), and (120) monoclinic phases of WO_3 [25]. The diffraction peaks stemming from the pure WO_3 align commendably with the hexagonal wurtzite structure as detailed in the JCPDS No. 75-2187 phase for WO_3, notably devoid of any traces of impurity peaks. Interestingly, the XRD spectra corresponding to the 3–5% La-doped WO_3 compounds mirror those of pure WO_3, displaying no discernible diffraction peaks. This outcome can be ascribed to the relatively low concentration of La introduced into the system and the consequent near-complete incorporation of La atoms within the crystalline framework of WO_3 [26]. This phenomenon underscores the subtle influence of the limited La doping on the overall crystallographic configuration of the WO_3 lattice.

3.2 Raman spectrum analysis

The Raman profiles of pure WO_3 and La-doped WO_3 samples in the 100–1,000 cm^{-1} range are shown in Figure 2. The highest strong band in Raman spectra was recorded at 807 cm^{-1} for all the studied samples. The band at 269 cm^{-1} is associated with υ(O–W–O) deformation vibrational bands, while the bands at 711 and 807 cm^{-1} are associated with (O–W–O) bending vibration modes of the molecule [27]. The obtained Raman peak profiles of WO_3 samples closely correspond to those already reported in the literature [28]. Also, there are no impurity-related bands observed, which encompasses the effective incorporation of the La ion into

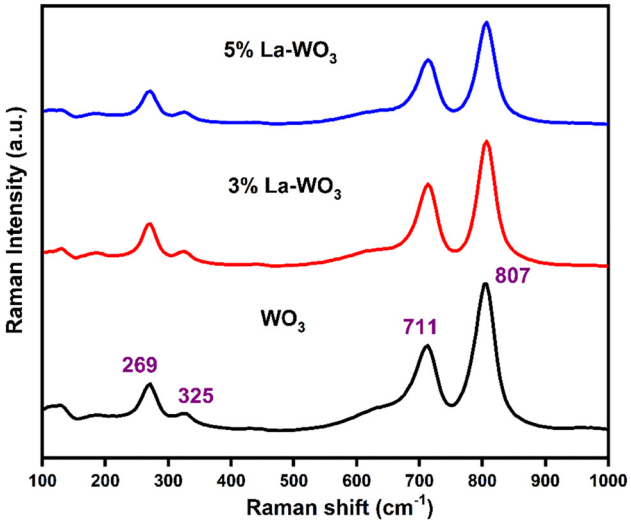

Figure 2: Raman pattern of pure WO_3 and La-doped WO_3 nanoparticles.

the WO_3 structure. The intensities of the peak decreases as the La concentration increases, indicating a decreased combination rate of light-induced charge carriers and an increase in oxygen vacancies [29].

3.3 Morphological features

3.3.1 FE-SEM analysis

The morphology of nanostructure materials is an important property because it usually dictates the performance of these materials. Figure 3(a) shows FE-SEM micrographs of pure and La-doped WO_3 samples. A homogeneous and agglomerated spherical morphology was observed [30]. The La dopant does not affect the morphology of the pure sample, but there is less aggregation of smaller round-shaped crystallites. The energy-dispersive X-ray spectra of La-doped WO_3 (5%) photocatalyst confirm the presence of La and WO_3 (Figure 3(b)).

3.4 Optical features

3.4.1 UV–visible absorbance analysis

UV–visible spectrophotometer is used to evaluate the optical properties and band gap energy of pure and La-doped WO_3 nanoparticles, as shown in Figure 4. With increasing La dopant concentration, La-doped WO_3 spectra show a red shift in the absorption edge. The distribution of charge density between the conduction or VB of La and WO_3 can result in a significant red shift [31]. The band gap energy of pure and La-doped WO_3 (3 and 5 wt%) were observed as 2.65, 2.52, and 2.46 eV, respectively. La-doped WO_3 samples showed a decreased band gap, which might be attributed to the formation of an intermediate energy level between the valance and conduction of pure WO_3. The decreased band gap energy of La-doped WO_3 may have potential applications in various industries [32].

The reduction in bandgap energy causes feasible electronic excitation within the materials upon UV–visible light absorption. As a result, the addition of La-doped WO_3 nanomaterials significantly improved the photocatalytic degradation of the MG dye. When La is doped with WO_3, the electrons present in the WO_3 readily excite from the VB to the CB. This transition occurs at very low energy, resulting in a favorable arrangement of energy levels between La and WO_3.

3.4.2 Photoluminescence analysis

The photogenerated charge carrier mitigation, transfer, and recombination in semiconductors were studied using the PL spectrum. Figure 5 depicts the PL spectrum of pure and La-doped WO_3 NPs at 320 nm. The maximum emission peak intensity of pure and La-doped WO_3 NPs is 485.9 nm, as seen in PL spectra [33]. The highest PL intensity is seen in pure WO_3, which can be altered by increasing the La concentration. The modest PL intensity of 5 wt% La-doped WO_3 NRs can cause defects/photogenerated electron–hole pair recombination. As a result, reducing the recombination rate of photogenerated charge carriers improved the effectiveness of photocatalytic dye degradation [34].

4 Photocatalysis application

4.1 MG dye degradation

The degradation of the MG dye under visible radiation is used to determine the photocatalytic performance of the samples. To prepare samples for photocatalytic examination, 0.1 g of MG is weighed. The photocatalytic reactor setup uses a 50 ppm solution of MG and 0.05 g of La-doped WO_3 catalyst. The solution is left in the dark for 60 min before being exposed to visible light [35]. The degraded dye sample is collected every 15 min and evaluated for dye degradation. The solution is then collected and analyzed using a UHS300 spectrophotometer to determine absorption spectra. The deterioration efficiency is calculated using the following formula [36]:

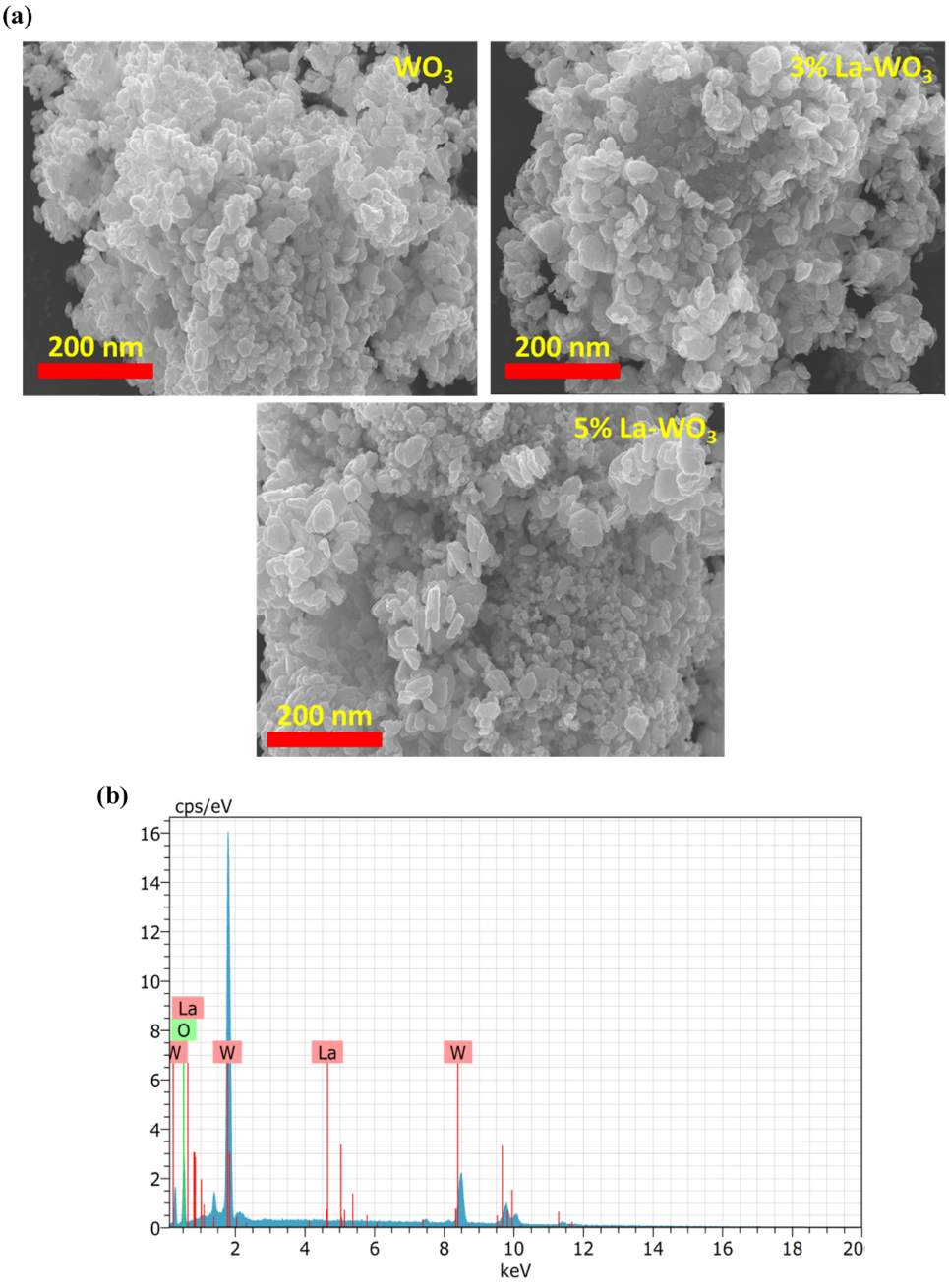

Figure 3: (a) FE-SEM spectra of pure WO_3 and La-doped WO_3 nanoparticles and (b) energy-dispersive X-ray spectroscopy spectrum of 5% La-doped WO_3 nanoparticles.

$$\text{Degradation efficiency} = \frac{A_0 - A(t)}{A_0} \times 100\%.$$

where A_0 represents the initial absorption of MG solution and $A(t)$ represents the absorption of different UV irradiation durations. Fundamentally, when exposed to visible light, every La-doped WO_3 emits electrons when its energy exceeds or equals the bandgap [37]. The presence of an equal amount of electrons and holes ($OH^{\cdot}$ and O_2^{-}) in the conduction and VB enables free radicals. Of course, all the samples demonstrated excellent dye molecule degradation (Figure 6(a) and (b)). La, with a concentration of 5%, yielded the greatest results, with an efficiency of 83.85%, compared to pure and 3% La-doped WO_3, which yielded degradation efficiencies of 81.16 and 83.11%, respectively.

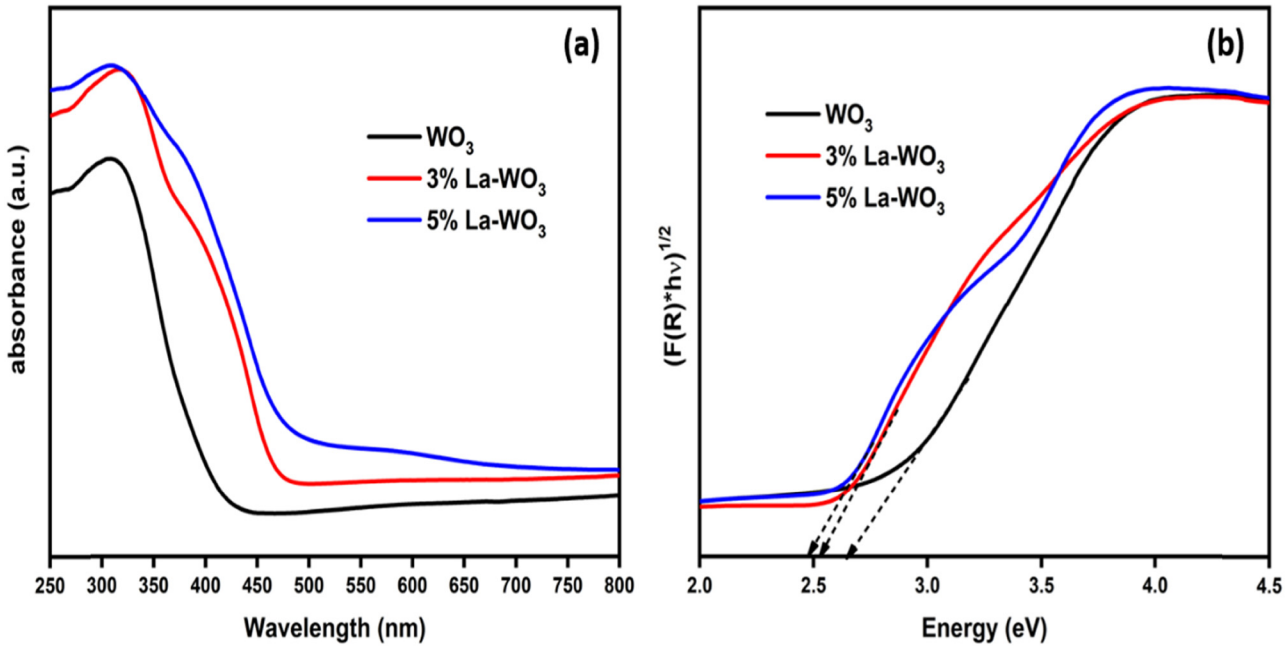

Figure 4: (a) UV–visible absorbance spectra and (b) TAUC plot of pure WO_3 and La-doped WO_3 nanoparticles.

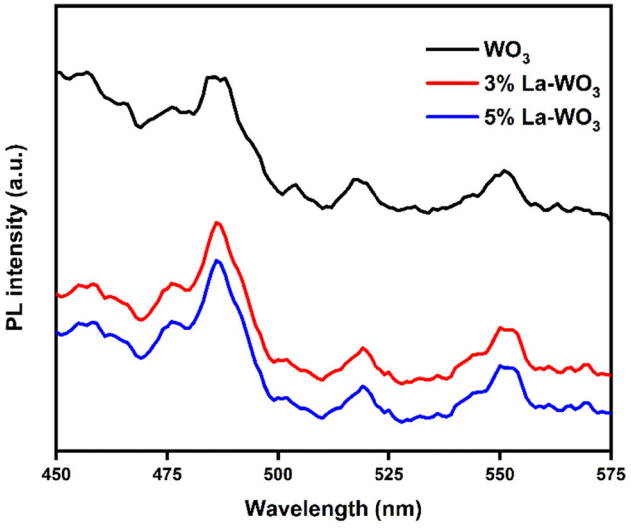

Figure 5: PL spectra of pure and La-doped WO_3 nanoparticles.

4.2 Photocatalytic mechanism

The mechanism of photocatalytic degradation generally involves several steps, which include [38]

- Adsorption and desorption of molecules,
- Formation of electron–hole pairs,
- Combination of electron–hole pairs, and
- Chemical reactions.

To be particular, the photocatalytic mechanism takes place in three important steps, and they are

- Adsorption of MG,
- Significant adsorption of photons, and
- Formation of oxidation and reducing species due to the charge transfer reactions.

In general, when light energy is radiated on the photocatalysts, electrons present in the valence shell of the photocatalyst excite to its CB. Because of the excitation, positive holes appear in the valence shell. These positive holes oxidize dye molecules converting them into highly reactive intermediates, resulting in a greater oxidation potential. If this reaction does not take place, then the positive holes react with water molecules to produce hydroxide radicals. Thus, by this process, dye degradation occurs.

Several works have been carried out by using different catalysts to increase the efficiency of the photocatalysis process. Particularly, in recent years, metal-oxide nanoparticles have been used as promising photocatalysts because of their low cost, abundance of raw material, and simple synthesizing method [39–41]. At the same time, the band gap of MO nanoparticles affects the photocatalytic activity (PCA). As the nanoparticles exhibit a narrow band gap, they tend to have the highest PCA.

The photodegradation of MG dye over La-doped WO_3 nanoparticles under visible radiation is displayed in Figure 7. When light is illuminated on a typical photocatalyst, the valence electrons acquire energy and are excited to the CB, and at the same time, holes are generated in the VB. Holes react with water molecules present in a dye solution to

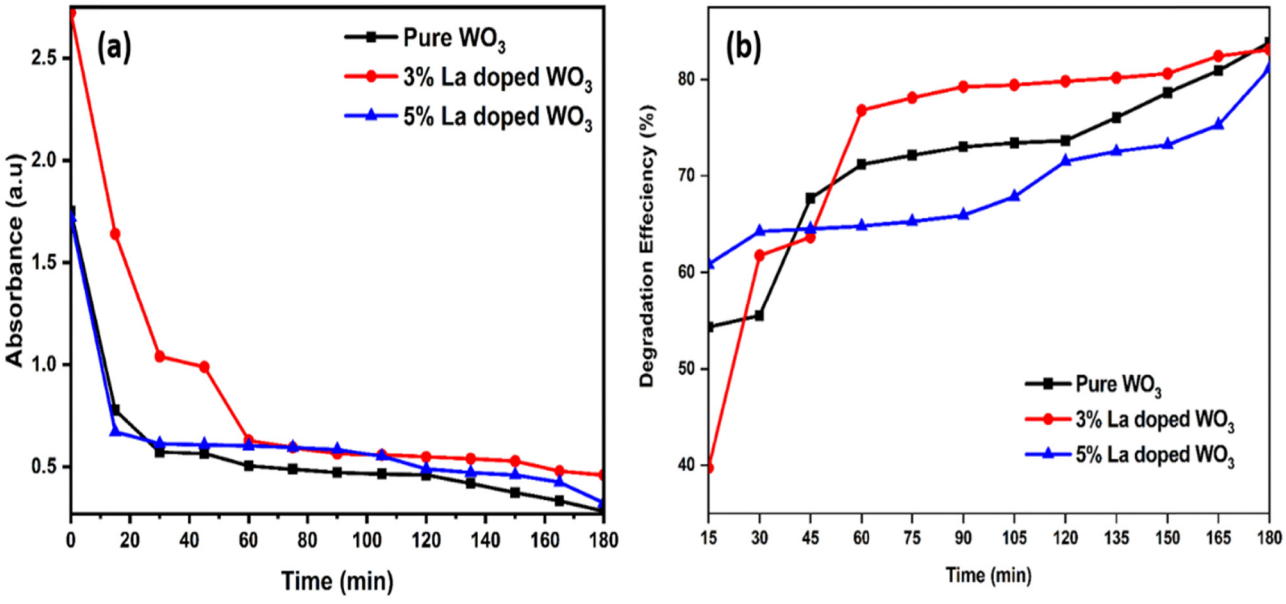

Figure 6: (a) UV–Vis absorbance plot and (b) photocatalytic degradation plot of pure WO_3 and La-doped WO_3 nanoparticles on degrading MG dye.

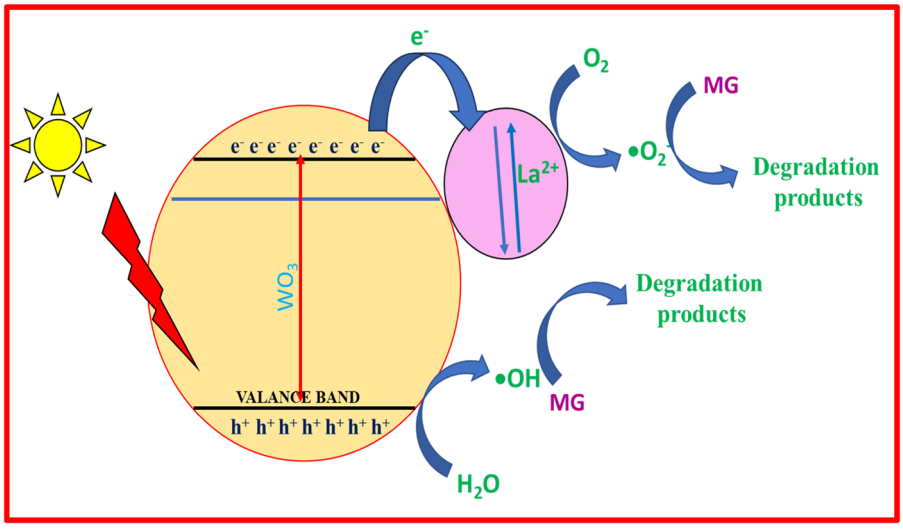

Figure 7: Photodegradation mechanism of MG dye under visible light irradiation.

create $OH^{\cdot}$ radicals [42]. On the contrary, additive La acts as an electron acceptor to accept the exited electron and delay the rate of photorecombination. The trapped electron reacts with oxygen molecules in water to form $^{\cdot}O_2^-$ radicals [43]. Free radicals $^{\cdot}OH$ and $^{\cdot}O_2^-$ initiate the MG dye degradation process under visible light irradiation. The process of photodegradation mechanism of MG dye is illustrated as follows:

$$WO_3 + h\nu \rightarrow WO_3 + (h^+ + e^-)$$

$$h^+ + H_2O \rightarrow {}^{\cdot}OH$$

$$La^{3+} + e^- \rightarrow La^{2+}$$

$$e^- + O_2 \rightarrow {}^{\cdot}O_2^-$$

$$\text{MG dye} + {}^{\cdot}OH/{}^{\cdot}O_2^- \rightarrow \text{degradation products}$$

Thus, it was identified that La-doped WO_3 nanoparticles can act as the best photocatalytic degradation of MG dye. Further, the stability and reusability of the synthesized catalyst can be studied by the few reported studies [44,45]. The adsorbed molecules can be removed by centrifuging at the speed of 1,200 rpm, followed by washing with

water and drying in a vacuum for 10 h. Once the degradation efficiency is reduced the process of centrifuging can be stopped.

5 Conclusion

The present work focused on a simple and efficient co-precipitation method for the synthesis of La-doped WO_3 nanoparticles, a heterojunction photocatalyst. Under visible light irradiation, the MG dye was totally destroyed on 5% La-doped WO_3 nanoparticles in 180 min. Furthermore, the photocatalytic efficiency for the degradation of MG dye using the 5% La-doped WO_3 nanoparticles was found to be greater than that of both pure WO_3 and 3% La-doped WO_3 nanoparticles. The enhanced photocatalytic performance is likely attributable to the three-dimensional hierarchical structure and the facilitated transition and separation of photogenerated electron–hole pairs in 5% La-doped WO_3, owing to the alignment of their respective band locations. Consequently, the 5% La-doped WO_3 photocatalysts proved to be excellent options for the degradation of organic pollutants, showcasing both high efficiency and stability under challenging conditions when exposed to visible light.

Acknowledgements: The authors extend their appreciation to the Researchers Supporting Project number (RSPD2024R999), King Saud University, Riyadh, Saudi Arabia.

Funding information: Research Supporting Project from King Saud University, Riyadh, Saudi Arabia.

Author contributions: Gokila Viswanathan – original draft preparation, writing, reviewing, and editing; Ayyappan Solaiappan – conceptualization, investigation, and formal analysis; Brindha Thirumalairaj – investigation, validation, reviewing, and formal analysis; Md. Irfanul Haque Siddiqui – investigation and formal analysis; Natrayan Lakshmaiya – reviewing and formal analysis; Umapathi Krishnamoorthy – supervision, editing, and reviewing; and Mohd Asif Shah – reviewing and formal analysis.

Conflict of interest: The authors declare no competing interests.

Data availability statement: Data sharing is not applicable to this article as no datasets were generated or analyzed during the current study.

Ethical approval: The conducted research is not related to either human or animal use.

References

[1] Ray S, Shaju ST. Bioaccumulation of pesticides in fish resulting toxicities in humans through food chain and forensic aspects. Environ Anal Health Toxicol. 2023 Aug;38(3):e2023017-7.

[2] Chojnacka K, Mikulewicz M. Bioaccumulation. Elsevier EBooks; 2014. p. 456–460, https://doi.org/10.1016/b978-0-12-386454-3.01039-3.

[3] Ghosh A, Tripathy A, Ghosh D. Impact of endocrine disrupting chemicals (EDCs) on reproductive health of human. Proceedings of the Zoological Society; 2022 Mar.

[4] Saravanan R, Sathish T, Sharma K, Rao AV, Sathyamurthy R, Panchal H, et al. Sustainable wastewater treatment by RO and hybrid organic polyamide membrane nanofiltration system for clean environment. Chemosphere. 2023;337:139336. doi: 10.1016/j.chemosphere.2023.139336

[5] Mohamad HA, Hemdan M, Bastawissi AA, Bastawissi AE, Panchal H, Sadasivuni KK. Industrial wastewater treatment by electrocoagulation powered by a solar photovoltaic system. Energy Sources, Part A: Recovery, Util Environ Eff. 2021;1–12. doi: 10.1080/15567036.2021.1950870.

[6] Chen D, Cheng Y, Zhou N, Chen P, Wang Y, Li K, et al. Photocatalytic degradation of organic pollutants using TiO2-based photocatalysts: A review. J Clean Prod. 2020 Sep;[cited 2020 Oct 31] 268:121725, https://www.sciencedirect.com/science/article/pii/S0959652620317728.

[7] Zhang C, Liu G, Geng X, Wu K, Debliquy M. Metal oxide semiconductors with highly concentrated oxygen vacancies for gas sensing materials: A review. Sens Actuators A: Phys. 2020 Jul;309:112026.

[8] Yuan Y, Guo R, Hong L, Ji X, Li Z, Lin Z, et al. Recent advances and perspectives of MoS2-based materials for photocatalytic dyes degradation: A review. Colloids Surf A: Physicochem Eng Asp. 2021 Feb;611:125836–6.

[9] Chidambaram S, Baskaran B, Ganesan M, Muthusamy S, Alavandar S, Muthusamy S, et al. One pot synthesis of Ag-Au/ZnO nanocomposites: a multi-junction component for sunlight photocatalysis. Energy Sources, Part A: Recovery, Util, Environ Eff. 2022;44(1):758–70. doi: 10.1080/15567036.2022.2050855

[10] Baruah S, Najam Khan M, Dutta J. Perspectives and applications of nanotechnology in water treatment. Environ Chem Lett. 2015 Nov;14(1):1–14.

[11] Fadillah G, Yudha SP, Sagadevan S, Fatimah I, Muraza O. Magnetic iron oxide/clay nanocomposites for adsorption and catalytic oxidation in water treatment applications. Open Chem. 2020 Sep;18(1):1148–66.

[12] Hu K, Kulkarni DD, Choi I, Tsukruk VV. Graphene-polymer nanocomposites for structural and functional applications. Prog Polym Sci. 2014 Nov;39(11):1934–72.

[13] Pallavi N, Rakshitha R, Chethan R. Photocatalytic removal of emerging contaminants from water using metal oxide-based nanoparticles. Curr Nanosci. 2024 May;20(3):339–55.

[14] Akter J, Hanif MdA, Islam MdA, Sapkota KP, Hahn JR. Selective growth of Ti3 +/TiO2/CNT and Ti3 +/TiO2/C nanocomposite for enhanced visible-light utilization to degrade organic pollutants by lowering TiO2-bandgap. Sci Rep. 2021 May;11(1).

[15] Dutta V, Sharma S, Raizada P, Thakur VK, Khan AAP, Saini V, et al. An overview on WO3 based photocatalyst for environmental remediation. J Environ Chem Eng. 2021 Feb;9(1):105018.

[16] Murillo-Sierra JC, Hernández-Ramírez A, Hinojosa-Reyes L, Guzmán-Mar JL. A review on the development of visible light-responsive WO3-based photocatalysts for environmental applications. Chem

Eng J Adv. 2021 Mar;[cited 2021 Oct 5] 5:100070, https://www.sciencedirect.com/science/article/pii/S2666821120300703.
[17] Shandilya P, Sambyal S, Sharma R, Mandyal P, Fang B. Properties, optimized morphologies, and advanced strategies for photocatalytic applications of WO3 based photocatalysts. J Hazard Mater. 2022 Apr;428:128218.
[18] Jiang Z, Cheng B, Zhang Y, Wageh S, Al-Ghamdi AA, Yu J, et al. S-scheme ZnO/WO3 heterojunction photocatalyst for efficient H2O2 production. J Mater Sci & Technol. 2022 Oct 1;124:193–201.
[19] Liao M, Su L, Deng Y, Xiong S, Tang R, Wu Z, et al. Strategies to improve WO3-based photocatalysts for wastewater treatment: a review. J Mater Sci. 2021 Jun;56(26):14416–47.
[20] Din MI, Tariq M, Hussain Z, Khalid R. Single step green synthesis of nickel and nickel oxide nanoparticles from Hordeum vulgare for photocatalytic degradation of methylene blue dye. Inorg Nano-Metal Chem. 2020 Jan;50(4):292–7.
[21] Din MI, Khalid R, Hussain Z. Minireview: silver-doped titanium dioxide and silver-doped zinc oxide photocatalysts. Anal Lett. 2017 Dec;51(6):892–907.
[22] Din MI, Najeeb J, Hussain Z, Khalid R, Ahmad G. Biogenic scale up synthesis of ZnO nano-flowers with superior nano-photocatalytic performance. Inorg Nano-Metal Chem. 2020 Feb;50(8):613–9.
[23] Sarathi R, Sundar SM, Jayamurugan P, Ganganagunta S, Sudhadevi D, Ubaidullah M, et al. Impacts of pH on photocatalytic efficiency, the control of energy and morphological properties of CuO nanoparticles for industrial wastewater treatment applications. Mater Sci Eng B. 2023 Dec 1;298:116856–6.
[24] Park JH, Kim S, Bard AJ. Novel carbon-doped TiO2 nanotube arrays with high aspect ratios for efficient solar water splitting. Nano Lett. 2005 Dec;6(1):24–8.
[25] Subramani T, Thimmarayan G, Balraj B, Narendhar C, Matheswaran P, Nagarajan SK, et al. Surfactants assisted synthesis of WO3 nanoparticles with improved photocatalytic and antibacterial activity: A strong impact of morphology. Inorg Chem Commun. 2022 Aug;142:109709–9.
[26] Zhang Y, Wu C, Xiao B, Yang L, Jiao A, Li K, et al. Chemo-resistive NO_2 sensor using La-doped WO3 nanoparticles synthesized by flame spray pyrolysis. Sens Actuators B: Chem. 2022 Oct;369:132247.
[27] Abbaspoor M, Aliannezhadi M, Tehrani FS. Effect of solution pH on as-synthesized and calcined WO3 nanoparticles synthesized using sol-gel method. Optical Mater. 2021 Nov;121:111552.
[28] Antony AJ, Jelastin M, Joel C, Bennie RB, Praveendaniel S. . Enhancing the visible light induced photocatalytic properties of WO_3 nanoparticles by doping with vanadium. J Phys Chem Solids. 2021 Oct;157:110169–9.
[29] Abbaspoor M, Aliannezhadi M, Tehrani FS. High-performance photocatalytic WO3 nanoparticles for treatment of acidic wastewater. J Sol-Gel Sci Technol. 2022 Nov;105(2):565–76.
[30] Shaheen N, Warsi MF, Zulfiqar S, Althakafy JT, Alanazi AK. Muhammad Imran Din, et al. La-doped WO3@gCN nanocomposite for efficient degradation of cationic dyes. Ceram Int. 2023 May;49(10):15507–26.
[31] Subramani T, Thimmarayan G, Balraj B, Narendhar C, Matheswaran P, Nagarajan SK, et al. Surfactants assisted synthesis of WO3 nanoparticles with improved photocatalytic and antibacterial activity: A strong impact of morphology. Inorg Chem Commun. 2022 Aug 1;142:109709.
[32] Kumari H, Sonia, Suman, Ranga R, Chahal S, Devi S, et al. A review on photocatalysis used for wastewater treatment: dye degradation. Water Air Soil Pollut. 2023 May;234(6):349.
[33] Mohan L, Avani AV, Kathirvel P, Marnadu R, Packiaraj R, JR, Joshua, et al. Investigation on structural, morphological and electrochemical properties of Mn doped WO3 nanoparticles synthesized by co-precipitation method for supercapacitor applications. J Alloy Compd. 2021 Nov;882:160670.
[34] Bhuvaneswari K, Palanisamy G, Bharathi G, Pazhanivel T, Upadhyaya IR, Kumari MLA, et al. Visible light driven reduced graphene oxide supported ZnMgAl LTH/ZnO/g-C3N4 nanohybrid photocatalyst with notable two-dimension formation for enhanced photocatalytic activity towards organic dye degradation. Environ Res. 2021 Jun;197:111079.
[35] Ebrahimi R, Maleki A, Zandsalimi Y, Ghanbari R, Shahmoradi B, Rezaee R, et al. Photocatalytic degradation of organic dyes using WO_3-doped ZnO nanoparticles fixed on a glass surface in aqueous solution. 2019 May;73:297–305.
[36] Verma M, Singh KP, Kumar A. Reactive magnetron sputtering based synthesis of WO3 nanoparticles and their use for the photocatalytic degradation of dyes. Solid State Sci. 2020 Jan;[cited 2022 Dec 22] 99:105847, https://www.sciencedirect.com/science/article/pii/S1293255818311440.
[37] Ghenaatgar A, A.Tehrani M, Khadir A. Photocatalytic degradation and mineralization of dexamethasone using WO3 and ZrO2 nanoparticles: Optimization of operational parameters and kinetic studies. J Water Process Eng. 2019 Dec;32:100969.
[38] Elkady MF, Hassan HS. Photocatalytic degradation of malachite green dye from aqueous solution using environmentally compatible Ag/ZnO polymeric nanofibers. Polymers. 2021 Jun;13(13):2033.
[39] Montañez JP, Pierella LB, Santiago AN. Photodegradation of herbicide dicamba with TiO2 immobilized on HZSM-11 Zeolite. Int J Environ Res. 2015 Oct;9(4):1237–44.
[40] McKeown NB, Budd PM. Polymers of intrinsic microporosity (PIMs): organic materials for membrane separations, heterogeneous catalysis and hydrogen storage. Chem Soc Rev. 2006;35(8):675.
[41] Singh P, Shandilya P, Raizada P, Sudhaik A, Rahmani-Sani A, Hosseini-Bandegharaei A. Review on various strategies for enhancing photocatalytic activity of graphene based nanocomposites for water purification. Arab J Chem. 2020 Jan;13(1):3498–520.
[42] Govindaraj T, Mahendran C, Chandrasekaran J, Manikandan VS, Shkir M, Massuod EE, et al. Effect of incorporation of La into WO_3 nanorods for improving photocatalytic activity under visible light irradiation. J Phys Chem Solids. 2022 Nov;170:110908.
[43] Chen P, Liang Y, Xu Y, Zhao Y, Song S. Synchronous photosensitized degradation of methyl orange and methylene blue in water by visible-light irradiation. J Mol Liq. 2021 Jul;334:116159.
[44] Govindaraj T, Mahendran C, Manikandan VS, Suresh R. One-pot synthesis of tungsten oxide nanostructured for enhanced photocatalytic organic dye degradation. J Mater Sci: Mater Electron. 2020 Sep;31(20):17535–49.
[45] Din MI, Khalid R, Hussain Z. Novel in-situ synthesis of copper oxide nanoparticle in smart polymer microgel for catalytic reduction of methylene blue. J Mol Liq. 2022 Jul;358:119181.